A precise determination of top quark electroweak couplings at the ILC operating at $\sqrt{s} = 500\,\mathrm{GeV}$

M.S. Amjad[1], M. Boronat[2], T. Frisson[1], I. Garcìa Garcìa[2], R. Pöschl[*,1], E. Ros[2], F. Richard[1,2], J. Rouëné[1] and M. Vos[2]

[1]LAL, CNRS/IN2P3, Université Paris Sud, F-91898 Orsay CEDEX, FRANCE
[2]IFIC, Universitat de Valencia CSIC, c/ Catedràtico José Beltràn, 2 46980 Paterna, SPAIN

Abstract

Top quark production in the process $e^+e^- \to t\bar{t}$ at a future linear electron positron collider with polarised beams is a powerful tool to determine the scale of new physics. The presented study assumes a centre-of-mass energy of $\sqrt{s} = 500\,\mathrm{GeV}$ and a luminosity of $\mathcal{L} = 500\,\mathrm{fb}^{-1}$ equality shared between the incoming beam polarisations of $P_{e^-,+} = \pm0.8, \mp0.3$. Events are selected in which the top pair decays semi-leptonically. The study comprises the cross sections, the forward-backward asymmetry and the slope of the helicity angle asymmetry. The vector, axial vector and tensorial CP conserving couplings are separately determined for the photon and the Z^0 component. The sensitivity to new physics would be dramatically improved w.r.t. to what expected from LHC for electroweak couplings.

1 Introduction

The top quark, or t quark, is by far the heaviest elementary particle of the Standard Model. Its large mass implies that this is the Standard Model particle that is most strongly coupled to the mechanism of electroweak symmetry breaking. For this

---

*Corresponding author: poeschl@lal.in2p3.fr

and other reasons, the t quark is expected to be a window to any new physics at the TeV energy scale. New physics will modify the electro-weak $t\bar{t}X$ vertex described in the Standard Model by *Vector* and *Axial* vector couplings V and A to the vector bosons $X = \gamma, Z^0$,

Generally speaking, an e^+e^- linear collider (LC) can measure t quark electroweak couplings at the % level. In contrast to the situation at hadron colliders, the leading-order pair production process $e^+e^- \rightarrow t\bar{t}$ goes directly through the $t\bar{t}Z^0$ and $t\bar{t}\gamma$ vertices. There is no concurrent QCD production of t quark pairs, which increases greatly the potential for a clean measurement. In the literature there a various ways to describe the current at the $t\bar{t}X$ vertex. The Ref. [1] uses

$$\Gamma_\mu^{ttX}(k^2,\, q,\, \overline{q}) = ie\left\{\gamma_\mu\left(\widetilde{F}_{1V}^X(k^2) + \gamma_5\widetilde{F}_{1A}^X(k^2)\right) + \frac{(q-\overline{q})_\mu}{2m_t}\left(\widetilde{F}_{2V}^X(k^2) + \gamma_5\widetilde{F}_{2A}^X(k^2)\right)\right\}.$$
(1)

with k^2 being the four momentum of the exchanged boson and q and $\overline{q}$ the four vectors of the t and $\bar{t}$ quark. Further γ_μ with $\mu = 0,..,3$ are the Dirac matrices describing vector currents and $\gamma_5 = i\gamma_0\gamma_1\gamma_2\gamma_3$ is the Dirac matrix allowing to introduce an axial vector current into the theory

The Gordon composition of the current reads

$$\Gamma_\mu^{ttX}(k^2, q, \overline{q}) = -ie\left\{\gamma_\mu\left(F_{1V}^X(k^2) + \gamma_5 F_{1A}^X(k^2)\right) + \frac{\sigma_{\mu\nu}}{2m_t}(q+\overline{q})^\mu\left(iF_{2V}^X(k^2) + \gamma_5 F_{2A}^X(k^2)\right)\right\},$$
(2)

with $\sigma_{\mu\nu} = \frac{i}{2}\left(\gamma_\mu\gamma_\nu - \gamma_\nu\gamma_\mu\right)$. The couplings or form factors $\widetilde{F}_i^X$ and F_i^X appearing in Eqs. 1 and 2 are related via

$$\widetilde{F}_{1V}^X = -\left(F_{1V}^X + F_{2V}^X\right), \qquad \widetilde{F}_{2V}^X = F_{2V}^X, \qquad \widetilde{F}_{1A}^X = -F_{1A}^X, \qquad \widetilde{F}_{2A}^X = -iF_{2A}^X. \quad (3)$$

Within the Standard Model the F_i have the following values:

$$F_{1V}^{\gamma,SM} = -\frac{2}{3},\; F_{1A}^{\gamma,SM} = 0,\; F_{1V}^{Z,SM} = -\frac{1}{4s_w c_w}\left(1 - \frac{8}{3}s_w^2\right),\; F_{1A}^{Z,SM} = \frac{1}{4s_w c_w}, \qquad (4)$$

with s_w and c_w being the sine and the cosine of the Weinberg angle θ_W. The coupling F_{2V}^γ is related via $F_{2V}^\gamma = Q_t(g-2)/2$ to the anomalous magnetic moment $(g-2)$ with Q_t being the electrical charge of the t quark. The coupling F_{2A} is related to the dipole moment $d = (e/2mt)F_{2A}(0)$ that violates the combined *C*harge and *P*arity symmetry CP. Note, that all the expressions above are given at Born level. Throughout the article no attempt will be made to go beyond that level.

Today, the most advanced proposal for a linear collider is the *I*nternational *L*inear *C*ollider, ILC [2,3], which can operate at centre-of-mass energies between about

0.1 TeV to 1 TeV. The ILC provides an ideal environment to measure these couplings. The $t\bar{t}$ pairs would be copiously produced, several 100,000 events at $\sqrt{s} = 500\,\text{GeV}$ for an integrated luminosity of $500\,\text{fb}^{-1}$. It is possible to almost entirely eliminate the background from other Standard Model processes. The ILC will allow for polarised electron and positron beams. With the use of polarised beams, t and $\bar{t}$ quarks oriented toward different angular regions in the detector are enriched in left-handed or right-handed t quark helicity [4]. This means that the experiments can independently access the couplings of left- and right-handed chiral parts of the t quark wavefunction to the Z^0 boson and the photon. In principle, the measurement of the cross section and forward-backward asymmetry A^t_{FB} for two different polarisation settings allows extracting both, the photon and Z^0 couplings of the t quark for each helicity state. This study introduces the angle of the decay lepton in semi-leptonic decays of the $t\bar{t}$ in the rest frame of the t quark. This angle will be called the *helicity angle*. The slope of the resulting angular distribution is a measure for the fraction of t quarks in left-handed helicity state, t_L and right-handed helicity state, t_R, in a given sample. There are therefore six independent observables

- The cross section;

- The forward backward asymmetry A^t_{FB};

- The slope of the distribution of the helicity angle;

for two beam polarisations. For the extraction of the six CP conserving form factors defined for the Z^0 and the photon, F_{1V}, F_{1A} and F_{2V}, the following observations have to be taken into account: Close to the $t\bar{t}$ threshold the observables depend always on the sum $F_{1V} + F_{2V}$. Therefore a full disentangling of the form factors will be unprecise for energies below about 1 TeV. Hence, in the present study either the four form factors $\widetilde{F}_1$ are varied simultaneously, while the two $\widetilde{F}_2$ are kept at their Standard Model values or vice versa.

This article is organised as follows. After this introduction the relations between the observables and the form factors are outlined before the experimental environment and the used data samples will be introduced. After that the selection of semi-leptonic decays of the $t\bar{t}$ pair will be presented and the selection efficiencies will be given. The determination of A^t_{FB} will be followed by the extraction of the slope of the distribution of the helicity angle.. This leads finally to the extraction of the six form factors as explained above. This study goes therefore beyond earlier studies published in [5,6].

2 Observables and Form Factors

According to [7], the cross section for any process in e^+e^- collisions in case of polarised beams can be written as

$$\sigma_{\mathcal{P},\mathcal{P}'} = \frac{1}{4}\left[(1 - \mathcal{P}\mathcal{P}')(\sigma_{-,+} + \sigma_{+,-}) + (\mathcal{P} - \mathcal{P}')(\sigma_{+,-} - \sigma_{-,+})\right] \tag{5}$$

In this equation the symbols $-$ and $+$ indicate full polarisation of the incoming beams with electrons and positrons of left-handed, L, or right-handed, R, helicity, respectively. The configurations $\sigma_{-,-}$ and $\sigma_{+,+}$ have been neglected due to helicity conservation at the electron vertex in the high energy limit. The degree of polarisation of the incoming beams is expressed by $\mathcal{P}$, for electrons, and $\mathcal{P}'$, for positrons.

In case of polarised beams Ref. [8] suggests to express the form factors introduced in Sec. 1 in terms of the helicity of the incoming electrons,

$$\mathcal{F}_{ij}^L = -F_{ij}^\gamma + \left(\frac{-\frac{1}{2} + s_w^2}{s_w c_w}\right)\left(\frac{s}{s - m_Z^2}\right)F_{ij}^Z$$

$$\mathcal{F}_{ij}^R = -F_{ij}^\gamma + \left(\frac{s_w^2}{s_w c_w}\right)\left(\frac{s}{s - m_Z^2}\right)F_{ij}^Z , \tag{6}$$

with $i = 1, 2$ and $j = V, A$ and m_Z being the mass of the Z^0 boson. The cross section for $t\bar{t}$ quark production for electron beam polarisation $I = L, R$ reads

$$\sigma_I = 2\mathcal{A}N_c\beta\left[(1 + 0.5\gamma^{-2})(\mathcal{F}_{1V}^I)^2 + (\mathcal{F}_{1A}^{I'})^2 + 3\mathcal{F}_{1V}^I\mathcal{F}_{2V}^I\right], \tag{7}$$

where $\mathcal{A} = \frac{4\pi\alpha^2}{3s}$ with the running electromagnetic coupling α and N_c is the number of quark colours. Furthermore γ and β are the Lorentz factor and the velocity, respectively. The term $\mathcal{F}_{1A}^{I'} = \beta\mathcal{F}_{1A}^I$ describes the reduced sensitivity to axial vector couplings near the $t\bar{t}$ production threshold. The cross sections at the Born level of the signal process $e^+e^- \to t\bar{t}$ and the main Standard Model background processes at a centre-of-mass energy of $500\,\mathrm{GeV}$ are summarised in Table 1.

The forward-backward asymmetry A_{FB}^t can be expressed as

$$(A_{FB}^t)_I = \frac{-3\mathcal{F}_{1A}^{I'}(\mathcal{F}_{1V}^I + \mathcal{F}_{2V}^I)}{2\left[(1 + 0.5\gamma^{-2})(\mathcal{F}_{1V}^I)^2 + (\mathcal{F}_{1A}^{I'})^2 + 3\mathcal{F}_{1V}^I\mathcal{F}_{2V}^I\right]}, \tag{8}$$

which in the Standard Model takes the values $(A_{FB}^t)_L = 0.38$ and $(A_{FB}^t)_R = 0.47$.

The fraction of right-handed tops is given by the following expression:

$$(F_R)_I = \frac{(\mathcal{F}_{1V}^I)^2(1 + 0.5\gamma^{-2}) + (\mathcal{F}_{1A}^{I'})^2 + 2\mathcal{F}_{1V}^I\mathcal{F}_{1A}^{I'} + \mathcal{F}_{2V}^I(3\mathcal{F}_{1V}^I + 2\mathcal{F}_{1A}^{I'}) - \beta\mathcal{F}_{1V}^I\mathfrak{Re}(\mathcal{F}_{2A}^I)}{2\left[(1 + 0.5\gamma^{-2})(\mathcal{F}_{1V}^I)^2 + (\mathcal{F}_{1A}^{I'})^2 + 3\mathcal{F}_{1V}^I\mathcal{F}_{2V}^I\right]}. \tag{9}$$

4

Channel	$\sigma_{unpol.}$ [fb]	$\sigma_{-,+}$ [fb]	$\sigma_{+,-}$ [fb]	$\mathrm{A_{LR}^{SM}}\%$
$t\bar{t}$	572	1564	724	36.7
$\mu\mu$	456	969	854	6.3
$\sum_{\mathrm{q=u,d,s,c}} q\bar{q}$	2208	6032	2793	36.7
$b\bar{b}$	372	1212	276	62.9
γZ^0	11185	25500	19126	14.2
WW	6603	26000	150	98.8
$Z^0 Z^0$	422	1106	582	31.0
$Z^0 WW$	40	151	8.7	89
$Z^0 Z^0 Z^0$	1.1	3.2	1.22	45

Table 1: *Unpolarised cross-sections and cross-sections at the Born level for 100% beam polarisation for signal and background processes. The last column gives the left right asymmetry as expected from the Standard Model.*

The values expected in the Standard Model are $(F_R)_L = 0.25$ and $(F_R)_R = 0.76$. The Eq. 9 contains a CP violating term proportional to $\mathfrak{Re}(\mathcal{F}_{2A}^I)$. This term will not be determined in ths present study but can also be precisely estimated using CP violating observables, see later in Tab. 5. This implies that CP conserving form factors can be fully disentangled without the assumption of CP conservation.

3 Experimental environment and data samples

The International Linear Collider is a proposal for a linear electron-positron accelerator at the TeV scale. For a detailed description of the machine the reader is referred to [2,3]. For the studies presented in this article it is important to emphasise that the machine can deliver polarised electron and positron beams. At a centre-of-mass energy of $\sqrt{s} = 500\,\mathrm{GeV}$ the envisaged degree of polarisation is 80% in case of electrons and 30% in case of positrons.

The ILD detector is designed as a detector for Particle Flow. This means that the jet energy measurement is based on the measurement of individual particles [9]. A detailed description of the current model of the ILD detector can be found elsewhere [10]. The z-axis of the right handed co-ordinate system is given by the direction of the incoming electron beam. Polar angles given in this note are defined with respect to this axis. The most important sub-detectors for this study are described in the following.

- The vertex detector consists of three double layers of silicon extending be-

tween $16\,\mathrm{mm}$ and $60\,\mathrm{mm}$ in radius and between $62.5\,\mathrm{mm}$ and $125\,\mathrm{mm}$ in z direction. It is designed for an impact parameter resolution of $\sigma_{r\phi} = \sigma_{rz} = 5 \oplus 10/(p\sin^{\frac{3}{2}}\theta)\,\mu\mathrm{m}$.

- The measurement of charged tracks is supported by an inner Silicon Tracker (SIT) in the central region and by a set of silicon disks in forward direction, i.e. towards large absolute values of $cos\theta$.

- The ILD detector contains a large Time Projection Chamber (TPC) with an inner sensitive radius of $395\,\mathrm{mm}$ and an outer sensitive radius of $1743\,\mathrm{mm}$. The half length in z is $2250\,\mathrm{mm}$. Recent simulation studies confirm that the momentum of charged particle tracks can be measured to a precision of $\delta(1/P_T) \sim 2 \times 10^{-5}\,\mathrm{GeV}^{-1}$. Here P_T denotes the transverse component of the three momentum P of the particles.

- The electromagnetic calorimeter is a SiW sampling calorimeter. Its longitudinal depths of $24\,\mathrm{X_0}$ allows for the complete absorption of photons with energies of up to 50 GeV as relevant for the studies here. The simulated energy resolution of the electromagnetic calorimeter is $\frac{\Delta E}{E} = 15\%/\sqrt{E\,[\mathrm{GeV}]}$

- The hadronic calorimeter surrounds the electromagnetic calorimeter and comprises 4.5 interaction length λ_I.

  Two proposals exist for the hadronic calorimeter. A semi-digital variant consisting of steel absorbers and gas RPC chambers with a pixel size of $1 \times 1\,\mathrm{cm}^2$ as active material. The second one features scintillating tiles with size of $3 \times 3\,\mathrm{cm}^2$ as active material. The latter option is employed in the present work.

3.1 Event generation and technical remarks

The events are generated with version 1.95 of the `WHIZARD` event generator [11,12] in the form of six fermion final states of which $t\bar{t}$ events form a subsample.

The generated events are then passed to the PYTHIA simulation program to generate parton shower and subsequent hadronisation. Events are selected for which the difference between the invariant masses of the three fermion systems forming a top from WHIZARD and the input t mass to WHIZARD of $174\,\mathrm{GeV}$ is smaller than $5\Gamma_t$. Here Γ_t is the total decay width of the t quark. By this only about 70% of the events generated by WHIZARD are recognised as $t\bar{t}$ events and treated accordingly. The following analysis is based on the described sub-selection of events.

The study has been carried out on a fully polarised sample. Realistic values of the beam polarisations at the ILC at $\sqrt{s} = 500\,\mathrm{GeV}$ are however $\mathcal{P}, \mathcal{P}' = \pm 0.8, \mp 0.3$.

The cross section and therefore its uncertainty scales with the polarisation according to Eq. 5. The observables A^t_{FB} and λ_t vary only very mildly with the beam polarisation. Again, the reduced cross section leads to a higher statistical error for non-fully polarised beams. This will be correctly taken into account in the uncertainty of the results.

Events corresponding to a luminosity of $250\,\mathrm{fb}^{-1}$ for each of the polarisation configurations were subject to a full simulation of the ILD detector and subsequent event reconstruction using the version ILD_o1_v05 of the ILC software. In Ref. [13] it was shown that the background can be nearly eliminated for the semi-leptonic final state (95% purity). Therefore at this stage none of the listed background processes are included in the analysis.

4   Event selection

The analysis starts out from the studies presented in detail in [13]. The samples analysed here contain background generated by beam beam interactions, so-called $\gamma\gamma$ background. No cut to remove this background is applied in this analysis. Such a study is left for future work. The produced $t(\bar{t})$-quark decays almost exclusively in to a bW pair. The b quark hadronises giving rise to a jet. The W boson can decay *hadronically* into light quarks, which turn into jets, or *leptonically* into a pair composed by a charged lepton and a neutrino. The *semi-leptonic process* is defined by events in which one W decays hadronically while the other one decays leptonically, i.e.

$$t\bar{t} \to (bW)(bW) \to (bqq')(b\ell\nu) \tag{10}$$

In the Standard Model the fraction of semi-leptonic final states in $e^+e^- \to t\bar{t}$ is about 43%. The charged lepton allows for the determination of the t quark charge. The t quark mass is reconstructed from the hadronically decaying W which is combined with one of the b-quark jets. In general leptons are identified using typical selection criteria. The lepton from the W boson decay is either the most energetic particle in a jet or has a sizeable transverse momentum w.r.t. neighboured jets. More specific the following criteria are applied

$$x_T = p_{T,lepton}/M_{jet} > 0.25 \quad \text{and} \quad z = E_{lepton}/E_{jet} > 0.6, \tag{11}$$

where E_{lepton} is the energy and $p_{T,lepton}$ the transverse momentum of the lepton within a jet with energy E_{jet} and mass M_{jet}. The decay lepton in case of e and μ can be identified with an efficiency of about 85%, where the selection has a tendency to reject low momentum leptons. The τ leptons can decay themselves into e or μ, which are collinear with the produced τ but have lower momentum than primary decay leptons.

Taking into account the τ leptons, the efficiency to identify the decay lepton is about 70%.

The identified lepton is removed from the list of reconstructed particles and the remaining final state is again clustered into four jets. Two of these must be identified as being produced by the b-quarks of the t quark decay. The b-likeness or b-tag is determined with the `LCFIPlus` package, which uses information of the tracking system as input. Secondary vertices in the event are analysed by means of the jet mass, the decay length and the particle multiplicity. The jets with the highest b-tag values are selected. As shown in Fig. 1 the higher b-tag value is typically 0.92 while the smaller one is still around 0.65.
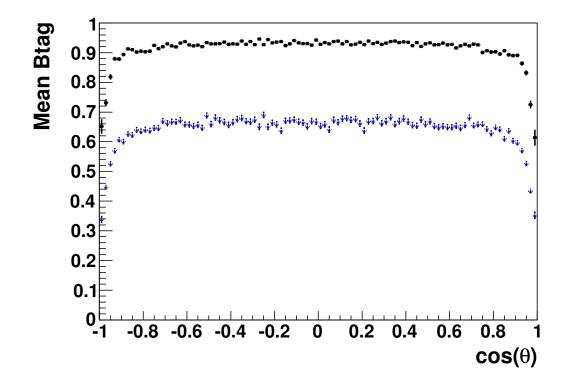

Figure 1: *The b-tag values as a function of the polar angle of the jets with the highest b-tag value (black dots) and of that with the second highest b-tag value (blue dots).*

These values are nearly independent of the polar angle of the b quark jet but drop towards the acceptance limits of the detector. Finally, the two remaining jets are associated with the decay products of the W boson. The signal is reconstructed by choosing that combination of b quark jet and W boson that minimises the following

equation:

$$d^2 = \left(\frac{m_{cand.} - m_t}{\sigma_{m_t}}\right)^2 + \left(\frac{E_{cand.} - E_{beam}}{\sigma_{E_{cand.}}}\right)^2 + \left(\frac{p_b^* - 68}{\sigma_{p_b^*}}\right)^2 + \left(\frac{cos\theta_{bW} - 0.23}{\sigma_{cos\theta_{bW}}}\right)^2 \quad (12)$$

In this equation $m_{cand.}$ and $E_{cand.}$ are invariant mass and energy of the t quark candidate decaying hadronically, respectively, and m_t and E_{beam} are input t mass and the beam energy of $250\,\mathrm{GeV}$. Beyond that it introduces the momentum of the b quark jet in the centre-of-mass frame of the t quark, p_b^* and the angle between the b quark and the W boson. The measured values are compared with the expected ones and the denominator is the width of the measured distributions. Distribution of latter two observables are shown in Fig. 2. Note, that the figure shows separately good and badly reconstructed events. This is explained in Sec. 5. Further cuts on jet thrust $T < 0.9$ and on the hadronic mass of the final state $180 < m_{had.} < 420\,\mathrm{GeV}$ are applied. In addition the mass windows for the reconstructed W-boson and t-quark are chosen to $50 < m_W < 250\,\mathrm{GeV}$ and $120 < m_t < 270\,\mathrm{GeV}$.

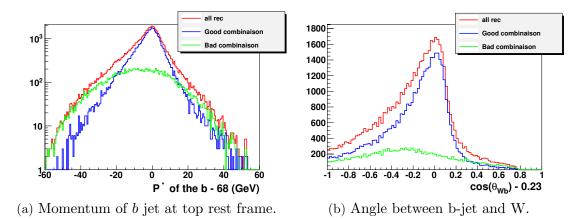(a) Momentum of b jet at top rest frame.   (b) Angle between b-jet and W.

Figure 2: *Distributions of the momentum of the b quark jet in the centre-of-mass frame of the t quark, p_b^* and the cosine of the angle θ_{bW} between the b quark and the W boson.*

The entire selection retains 53.5% signal events for the configuration $\mathcal{P}, \mathcal{P}' = -1, +1$ and 56.5% for the configuration $\mathcal{P}, \mathcal{P}' = +1, -1$.

5   Measurement of the forward backward asymmetry

Garcìa For the determination of the forward-backward asymmetry A_{FB}^t, the number of events in the hemispheres of the detector w.r.t. the polar angle θ of the t quark

is counted, i.e.

$$A_{FB}^t = \frac{N(\cos\theta > 0) - N(\cos\theta < 0)}{N(\cos\theta > 0) + N(\cos\theta < 0)}. \tag{13}$$

Here, the polar angle of the t quark is calculated from the decay products in the hadronic decay branch. The direction measurement depends on the correct association of the b quarks to the jets of the hadronic b quark decays. The analysis is carried out separately for a left-handed polarised electron beam and for a right handed polarised beam. Therefore, two different situations have to be distinguished, see also Fig. 3:

- In case of a *right*-handed electron beam the sample is expected to be enriched with t-quarks with *right*-handed helicity [4]. Due to the $V - A$ structure of the standard model an energetic W boson is emitted into the flight direction of the t-quark. The W boson decays into two energetic jets. The b quark from the decay of the t quark are comparatively soft. Therefore, the direction of the t quark is essentially reconstructed from the direction of the energetic jets from the W boson decay. This scenario is thus insensitive towards a wrong association of the jet from the b quark decay to the jets from the W boson decay

- In case of a *left*-handed electron beam the sample is enriched with t quarks with *left*-handed helicity. In this case the W boson is emitted opposite to the flight-direction of the t quark and gains therefore only little kinetic energy. In fact for a centre-of-mass energy of $500\,\mathrm{GeV}$ the W boson is nearly at rest. On the other hand the b quarks are very energetic and will therefore dominate the reconstruction of the polar angle of the t quark. In this case a wrong association of the jets with that from the b quark can flip the reconstructed polar angle by π giving rise to migrations in the polar angle distribution of the t quark.

The explanations above apply correspondingly to polarised positron beams and $\bar{t}$-quarks.

Figure 3: *In case of a t_R decay, the jets from the W dominate the reconstruction of the polar angle of the t quark. In case of a t_L the W is practically at rest and jets from the b quark dominate the and reconstruction of the polar angle of the t quark.*

10

The described scenarios are encountered as shown in Figure 4. First, the reconstructed spectrum of polar angles of the t quark in the case of right handed electron beams is in resonable agreement with the generated one. On the other hand the reconstruction of $\cos\theta_t$ in case of left-handed t quarks suffers from considerable migrations. As discussed, the migrations are caused by a wrong association of jets stemming from b quarks to jets stemming from W decays. This implies that the reconstruction of observables will get deteriorated. This implication motivates to restrict the determination of A^t_{FB} in case of $\mathcal{P}, \mathcal{P}' = -1, +1$ to cleanly reconstructed events as already studied previously in [14,15].
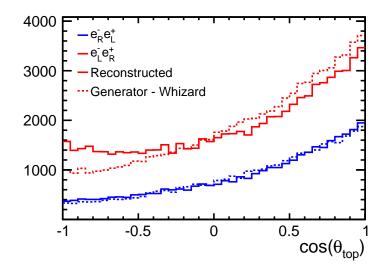

Figure 4: *Reconstructed forward backward asymmetry compared with the prediction by the event generator WHIZARD for two configurations of the beam polarisations.*

The quality of the reconstructed events is estimated by the following quantity

$$\chi^2 = \left(\frac{\gamma_t - 1.435}{\sigma_{\gamma_t}}\right)^2 + \left(\frac{E_b^* - 68}{\sigma_{E_b^*}}\right)^2 + \left(\frac{cos\theta_{bW} - 0.26}{\sigma_{cos\theta_{bW}}}\right)^2 \tag{14}$$

The observables p_b^* and $cos\theta_{bW}$ have already been introduced in Sec. 4. The defined χ^2 comprises in addition the Lorentz factor $\gamma_t = E_t/M_t$ of the final state t quark, which is shown in Figure 5. The correct association of the of jets from b quarks to that from W bosons is checked with the MC truth information Events in which this association went wrong, labelled as *bad combination* in Figs. 2 and 5, lead to a distorted distribution in these observables.
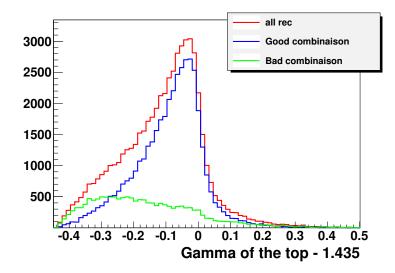
11

Figure 5: *Lorentz factor of the top to define the quantity* χ^2, *see Eq. 14, for the selection of well reconstructed events in case of* $\mathcal{P}, \mathcal{P}' = -1, +1$ *beam polarisation.*

For $\chi^2 < 15$ the reconstructed spectrum agrees very well with the generated one. For this cut on χ^2, the reconstruction efficiency is 27.6%. The Fig. 6 demonstrates the improved agreement between the reconstructed and generated direction of the t quark direction in case $\mathcal{P}, \mathcal{P}' = -1, +1$. The forward-backward asymmetry A_{FB}^t can be derived from these angular distributions. For completeness it has to be noted that effects of beam related $\gamma\gamma$ background on the angular distribution have been studied. The reconstruction of the angular distribution works better without these effects. The detailed treatment and quantification of these effects is left for further studies.

The numerical results are given in Tab. 2 and compared with the generated value. The statistical error is corrected for the realistic beam polarisations $\mathcal{P}, \mathcal{P}' = \pm 0.8, \mp 0.3$. It shows that for the standard luminosity statistical precisions of better than 2% can be expected. When selecting well reconstructed events the systematic error due to the ambiguities is expected to be significantly smaller than the statistical error.

$\mathcal{P}, \mathcal{P}'$	$(A_{FB}^t)_{gen.}$	A_{FB}^t	$(\delta_{A_{FB}}/A_{FB})_{stat.}$ [%]
$-1, +1$	0.360	0.359	1.7 (for $\mathcal{P}, \mathcal{P}' = -0.8, +0.3$)
$+1, -1$	0.433	0.410	1.3 (for $\mathcal{P}, \mathcal{P}' = +0.8, -0.3$)

Table 2: *Statistical precisions expected for* A_{FB}^t *for different beam polarisations.*
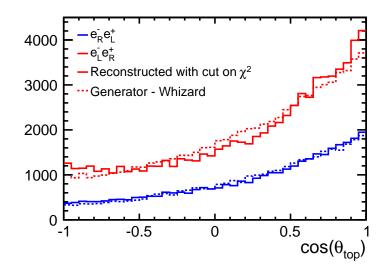
Figure 6: *Reconstructed forward backward asymmetry compared with the prediction by the event generator WHIZARD after the application of a on $\chi^2 < 15$ for the beam polarisations $P, P' = -1, +1$ as explained in the text. Note that no correction is applied for the beam polarisations $\mathcal{P}, \mathcal{P}' = +1, -1$*

6 Determination of the slope of the helicity angle distribution

The helicity approach has been suggested for top studies at Tevatron [16]. In the rest system of the t quark, the angle of the lepton from the W boson is distributed like:

$$\frac{1}{\Gamma}\frac{d\Gamma}{dcos\theta_{hel}} = \frac{1 + \lambda_t cos\theta_{hel}}{2} = \frac{1}{2} + (2F_R - 1)\frac{cos\theta_{hel}}{2}$$

$$\lambda_t = 1 \text{ for } t_R \quad \lambda_t = -1 \text{ for } t_L \tag{15}$$

This angular distribution is therefore linear and very contrasted between t_L and t_R. In practice there will be a mixture of t_R and t_L (beware that here L and R mean left and right handed helicities) and λ_t will have a value between -1 and +1 depending on the composition of the t quark sample.

According to [16], the angle θ_{hel} is measured in the rest frame of the t quark with the z-axis defined by the direction of motion of the t quark in the laboratory. As discussed in [4] this definition of θ_{hel} is not unique but some detailed investigations not

13

reproduced in this note have shown that the choice of [16] seems optimal. The observable $\cos\theta_{hel}$ is computed from the momentum of the t quark decaying semi-leptonically into a lepton, a b quark and a neutrino. If ISR effects (with the photon lost in the beam pipe) are neglected, one can simply assume energy momentum conservation. This, by means of the energy-momentum of the t quark decaying hadronically, allows for deducing the energy-momentum of the t quark decaying semi-leptonically. A Lorentz transformation boosts the lepton into the rest system of the t quark. This should give a very precise knowledge of $\cos\theta_{hel}$. To determine the helicity angle only the angle of the lepton needs to be known. For the leptonic decays of the τ lepton, which significantly contribute to this analysis (10-15%), the charged lepton and the τ lepton are approximately collinear and therefore the method remains valid.

6.1 Analysis of the helicity angle distribution

Based on the selection introduced in Sec. 4 the angular distribution of the decay lepton in the rest frame of the t quark is shown in Fig. 7 for fully polarised beams.
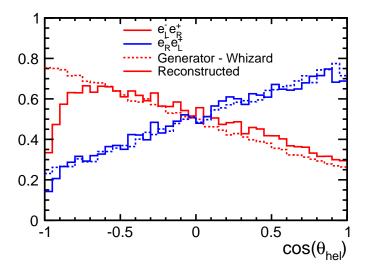

Figure 7: *Polar angle of the decay lepton in the rest frame of the t quark.*

The distribution exhibits a drop in reconstructed events towards $\cos\theta_{hel} = -1$. This drop can be explained by the event selection which suppresses leptons with small energies. Outside this region and in contrast to e.g. the forward-backward asymmetry the reconstructed angular distribution agrees very well with the generated one. This means that this observable suffers much less from the migration effect described in Sec. 5. It is therefore not necessary to tighten the selection in the same way as

for A_{FB}^t. The reason for the bigger robustness of the angular distribution can be explained by kinematics.

As outlined in Sec. 5 the migrations described there are provoked mainly by longitudinally polarised, *soft* W bosons from the decay of left handed t quarks. The W_L boson decay proportional to $\sin^2\theta$. Therefore any boost into the rest frame of the top leads predominantly to leptons with $\cos\theta_{hel} < 0$.

The parameter λ_t can be derived from the slope of the helcity angle distribution that is obtained by a fit to the linear part of the angular distribution in the range $\cos\theta_{hel} = [-0.6, 0.9]$. The results are summarised in Table 3 for the two initial beam polarisations $\mathcal{P} = \pm 1$ and $\mathcal{P}' = \mp 1$, where the statistical error is given for $\mathcal{P}, \mathcal{P}' = \mp 0.8, \pm 0.3$. The results are compared with the values of λ_t as obtained for the generated sample. A quarter of shift between the generated and the reconstructed value is taken into account for the systematic error of the measurement. The result changes by about 1% when changing the fit range to $\cos\theta_{hel} = [(-0.4, 0.5), 0.9]$. The errors on the slope from the variation of the fit range and that from the difference between generated and reconstructed slope are added in quadrature.

$\mathcal{P}, \mathcal{P}'$	$(\lambda_t)_{gen.}$	$(\lambda_t)_{rec.}$	$(\delta\lambda_t)_{stat.}$ for $\mathcal{P}, \mathcal{P}' = \mp 0.8, \pm 0.3$	$(\delta\lambda_t)_{syst.}$
$-1, +1$	-0.514	-0.476	0.011	0.011
$+1, -1$	0.546	0.510	0.016	0.010

Table 3: *Results on λ_t derived from the slope of the helicity angle distribution with errors for different beam polarisations at the ILC.*

7 Discussion of systematic uncertainties

In the previous sections measurements of either cross sections or asymmetries have been presented. This section makes an attempt to identify and quantify systematic uncertainties, which may influence the precision measurements.

- Luminosity: The luminosity is a critical parameter for cross section measurements only. The luminosity can be controlled to 0.1% [17].

- Polarisation: The polarisation is a critical parameter for all analyses. It enters directly the cross section measurements. The studies for the DBD using W pair production [18] lead to an uncertainty of 0.1% for the polarisation of the

electron beam and to an uncertainty of 0.35% for the polarisation of the positron beam. This translates into an uncertainty of 0.25% on the cross section for $\mathcal{P}, \mathcal{P}' = -0.8, +0.3$ and 0.18% on the cross section for $\mathcal{P}, \mathcal{P}' = +0.8, -0.3$ The uncertainty on the polarisation can be neglected with respect to the statistical uncertainty for A_{FB}^t and λ_t.

- Migrations: It has been shown in Sec. 5 that migrations have to be taken into account for the measurement of A_{FB}^t, in particular for the polarisations $\mathcal{P}, \mathcal{P}' = -1, +1$. These migrations are reduced by stringent requirements on the event selection using a χ^2 analysis. This in turn leads to a penalty in the efficiency. The success of the method depends in addition on a very sharp measurement of the variables used for the χ^2 analysis. A review of the procedure to handle the ambiguities will however be made in future studies. In the ideal case the ambiguities can be eliminated by a proper measurement of the charge of the b quark from the t decay.

- Other experimental effects: There is a number of other experimental effects imaginable like acceptance, uncertainties of the b tagging or the influence passive material. These effects depend on the experimental conditions that will really be encountered. The LEP experiments quote a systematic uncertainty on R_b of 0.2% a value which may serve as a guiding line for values to be expected at the ILC.

- Theory: The analysis performed here considers only the Born-level $t\bar{t}$ production diagrams. The electroweak corrections have been estimated in Ref. [19] and QCD corrections in [20]. Even if the corrections themselves are sizeable, the theoretical uncertainty on the total and differential production rate is not expected to dominate over the experimental uncertainties. A further complication arises from several other processes that yield the same final state. Single top production at the LC in association with a W boson and bottom quark (through WW^* production) leads to the same final state as t quark pair production. The interference between single t and t quark pair production processes is sizeable and must be taken into account in a realistic experimental strategy. This is left for a future study.

As a summary it can be concluded that the total systematic uncertainties will not exceed the statistical uncertainties. This, however, requires an excellent control of a number of experimental quantities on which the results depend.

Coupling	SM value	LHC [1] $\mathcal{L} = 300$ fb^{-1}	e^+e^- [6] $\mathcal{L} = 300$ fb^{-1} $\mathcal{P}, \mathcal{P}' = -0.8, 0$	e^+e^-[ILC DBD] $\mathcal{L} = 500$ fb^{-1} $\mathcal{P}, \mathcal{P}' = \pm0.8, \mp0.3$
$\Delta\widetilde{F}_{1V}^{\gamma}$	0.66	$+0.043$ -0.041	$-$ $-$	$+0.002$ -0.002
$\Delta\widetilde{F}_{1V}^{Z}$	0.23	$+0.240$ -0.620	$+0.004$ -0.004	$+0.002$ -0.002
$\Delta\widetilde{F}_{1A}^{Z}$	-0.59	$+0.052$ -0.060	$+0.009$ -0.013	$+0.006$ -0.006
$\Delta\widetilde{F}_{2V}^{\gamma}$	0.015	$+0.038$ -0.035	$+0.004$ -0.004	$+0.001$ -0.001
$\Delta\widetilde{F}_{2V}^{Z}$	0.018	$+0.270$ -0.190	$+0.004$ -0.004	$+0.002$ -0.002

Table 4: *Sensitivities achievable at 68.3% CL for CP conserving form factors $\widetilde{F}_{1V,A}^{X}$ and $\widetilde{F}_{2V}^{X}$ defined in Eq. 1 at the LHC and at linear e^+e^- colliders. The assumed luminosity samples and, for e^+e^- colliders, the beam polarisation, are indicated. In the LHC studies and in earlier studies for a linear e^+e^- collider as published in the TESLA TDR [6] study, only one coupling at a time is allowed to deviate from its Standard Model value. In the present study, denoted as ILC DBD, either the four form factors $\widetilde{F}_1$ or the two form factors $\widetilde{F}_2$ are allowed to vary independently. The sensitivities are based on statistical errors only.*

8 Interpretation of results

The results on the reconstruction efficiency, A_{FB}^t and λ_t presented in the previous sections are transformed into precisions on the form factors $\widetilde{F}_i$. The results are summarised in Table 4 and Figure 8 and are compared with results of earlier studies for a linear e^+e^- collider as published in the TESLA TDR [6] as well as with precisions expected for the LHC. For completeness, Tab. 5 compares sensitivites expected at the LHC with the results from the TESLA TDR [6] for CP violating form factors not calculated in the present study. Note, that in the LHC and TESLA studies only one form factor was varied at a time while in the present study two or four form factors are varied simultaneously, see Sec. 1. It is obvious that the measurements at an electron positron collider lead to a spectacular improvement and thus allow for a profound discussion of effects of new physics. Two examples are given in the following.

8.1 An example: The Randall-Sundrum scenario

The sensitivity new physics can be parameterised by general dimension six operators contributing to the $t\bar{t}\gamma$ and $t\bar{t}Z^0$ vertex [21]. However, the potential of the ILC might be demonstrated more clearly by presenting a concrete example with one particular model. In the original model of Randall and Sundrum [22] there are additional massive gauge bosons in an assumed extra dimension. The model predicts increased
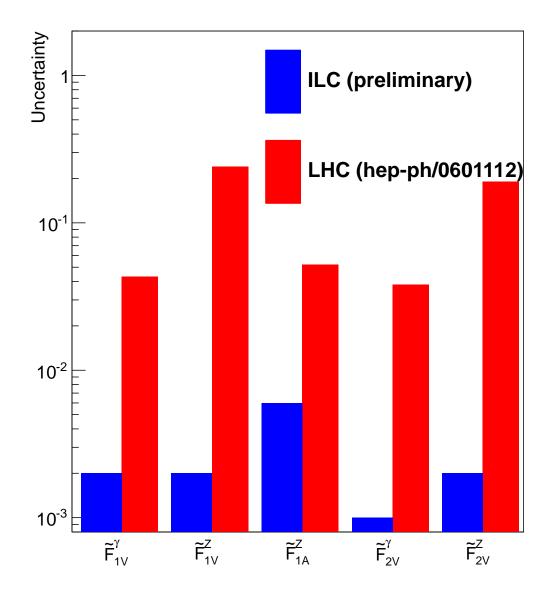
Figure 8: *Comparison of statistical precisions on CP conserving form factors expected at the LHC, taken from [1] and at the ILC. The LHC results assume an integrated luminosity of $\mathcal{L} = 300$ fb^{-1}. The results for ILC assume an integrated luminosity of $\mathcal{L} = 500$ fb^{-1} at $\sqrt{s} = 500$ GeV and a beam polarisation $\mathcal{P} = \pm 0.8, \mathcal{P}' = \mp 0.3$.*

Coupling	LHC [1] $\mathcal{L} = 300$ fb^{-1}	e^+e^- [6] $\mathcal{L} = 300$ fb^{-1} $\mathcal{P}, \mathcal{P}' = -0.8, 0$
$\Delta \mathrm{Re}\, \widetilde{F}_{2A}^{\gamma}$	$+0.17$ -0.17	$+0.007$ -0.007
$\Delta \mathrm{Re}\, \widetilde{F}_{2A}^{Z}$	$+0.35$ -0.35	$+0.008$ -0.008
$\Delta \mathrm{Im}\, \widetilde{F}_{2A}^{\gamma}$	$+0.17$ -0.17	$+0.008$ -0.008
$\Delta \mathrm{Im}\, \widetilde{F}_{2A}^{Z}$	$+0.035$ -0.035	$+0.015$ -0.015

Table 5: *Sensitivities achievable at 68.3% CL for the top quark magnetic and electric dipole form factors $\widetilde{F}_{2V}^{V}$ defined in Eq. 1, at the LHC and at for a linear e^+e^- collider as published in the TESLA TDR [6]. The assumed luminosity samples and, for TESLA, beam polarisation, are indicated. In the LHC study and in the TESLA study only one coupling at a time is allowed to deviate from its Standard Model value. The sensitivities are based on statistical errors only*

couplings of the t quark, and perhaps also the b quark, to these Kaluza-Klein particles. Following the analysis in [23,24,25], one can fix the parameters of the model so that these enhancements fit the two anomalies observed in the forward-backward asymmetry for b quarks A_{FB}^b at LEP1 and for t quarks A_{FB}^t at the Tevatron. This gives a viable model of t quark interactions associated with top and Higgs compositeness. Figure 9 shows the expected modifications of the helicity angle distributions within this scenario for a Kaluza-Klein mass of $M_{KK} = 2$ TeV. Staying within the framework of the Randall-Sundrum model, the ILC at $\sqrt{s} = 500$ GeV can observe more than three standard deviations on t quark couplings for masses of Kaluza-Klein particles of up to 50 TeV.

8.2 The anomalous magnetic moment $(g - 2)_t$

The determination of $\widetilde{F}_{2V}^{\gamma}$ gives access to anomalous magnetic moment $(g - 2)_t$ in a rather simple way. For instance $\widetilde{F}_{2V}^{\gamma} = Q_t(g - 2)_t/2$. $(g - 2)_t$ receives Standard Model contributions from QED, QCD and electroweak interactions [26]. One sees that this quantity will be measured to about 10% accuracy.

What is known about $(g - 2)_t$? In Ref. [27] it said that the limits on g_t come from the reaction $b \to s\gamma$ giving a very crude constraint :

$$- 3.5 < g_t < 3.6 \tag{16}$$

The expected precision on $(g - 2)_t/2$ of 0.1% is proportional to m_t/M where M is the scale of compositeness. It follows hence that with the accuracy expected at the ILC the compositeness of the t quark can be tested up to about 100 TeV.
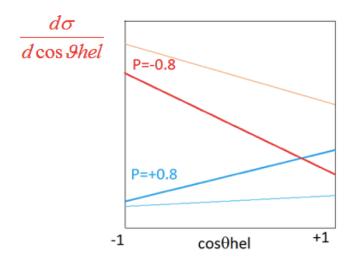
Figure 9: *Distributions of the helicity angle* $\cos\theta_{hel}$ *expected from the Standard Model (thick lines) and their modifications by the Randall-Sundrum framework (thin lines) described in the text. The results are shown for beam polarisations of* $\mathcal{P}, \mathcal{P}' = \pm 0.8, \mp 0.3.$

9 Summary and outlook

This article presents a comprehensive analysis of $t\bar{t}$ quark production using the semi-leptonic decay channel. Results are given for a centre-of-mass energy of $\sqrt{s} = 500\,\mathrm{GeV}$ and an integrated luminosity of $\mathcal{L} = 500\,\mathrm{fb}^{-1}$ shared equally between the beam polarisations. $P = \pm 0.8$ and $P' = \mp 0.3$.

Semi-leptonic events, including those with τ leptons in the final state can be selected with an efficiency of about 55%. The cross section of the semi-leptonic channel of $t\bar{t}$ quark production can therefore be measured to a statistical precision of about 0.5%. The second observable is the forward-backward asymmetry A^t_{FB}. It was shown that in particular for predominantly left handed polarisation of the initial electron beam the $V - A$ structure leads to migrations, which distort the theoretical expected A^t_{FB}. These migrations can be remedied by tightening the selection criteria of the events. Taking into account this correction the forward-backward asymmetry can be determined to a precision of better than 2% for both beam polarisations. Finally, the study introduced the slope of the helicity angle distribution, which is a new observable for ILC studies. This observable measures the fraction of t quarks of a given helicity in the event sample. This variable is very robust against e.g. the migration effects and can be measured to a precision of about 4%.

The observables together with the unique feature of the ILC to provide polarised

beams allow for a largely unbiased disentangling of the individual couplings of the t quark to the Z^0 boson and the photon. These couplings can be measured with high precision at the ILC and always more than one order of magnitude better than it will be possible at the LHC with $\mathcal{L} = 300\,\mathrm{fb}^{-1}$. This precision would allow for the verification of a great number of models for physics beyond the Standard Model. Examples for these models are extra dimensions and compositeness. The current analysis allows in the future to define observables to e.g. measure CP violation or to test other theoretical models. They constitute therefore a perfect basis for discussions with theoretical groups.

It has to be noted that the results contain only partially experimental systematical errors. These will have to be estimated in future studies. From the achieved precision it is mandatory that systematics are controlled to the 1% level or better in particular for the measurement of the cross section.

References

[1] A. Juste *et al.*, "Report of the 2005 Snowmass top/QCD working group" *ECONFC0508141:PLEN0043* (2005) , arXiv:hep-ph/0601112.

[2] **ILC Global Design Effort and World Wide Study**, N. Phinney, N. Toge, and N. Walker, eds., *ILC Reference Design Report Volume 3 - Accelerator.* 2007. arXiv:0712.2361 [physics.acc-ph]. ILC-REPORT-2007-001.

[3] "ILC TDR". https://forge.linearcollider.org/tdr.

[4] S. J. Parke and Y. Shadmi, "Spin correlations in top quark pair production at e^+e^- colliders" *Phys.Lett.* **B387** (1996) 199, arXiv:9606419 [hep-ph].

[5] **American Linear Collider Working Group Collaboration**, T. Abe *et al.*, "Linear Collider Physics Resource Book for Snowmass 2001 - Part 3" arXiv:hep-ex/0106057.

[6] R. D. Heuer, D. J. Miller, F. Richard and P. M. Zerwas (eds.), "Tesla technical design report part iii: Physics at an e^+e^- linear collider" arXiv:hep-ph/0106315.

[7] G. Moortgat-Pick *et al.*, "The role of polarized positrons and electrons in revealing fundamental interactions at the linear collider" *Phys.Rept.* **460 (2008) 131**, arXiv:hep-ph/0507011.

[8] C. Schmidt, "Top quark production and decay at next-to-leading order in e^+e^- annihilation" *Phys.Rev.* **D54 (1996) 3250**, arXiv:hep-ph/9504434.

[9] J. C. Brient and H. Videau, "The calorimetry at the future e^+e^- linear collider" *eConf* (2001) no. C010630, E3047, arxiv:hep-ex/0202004v1.

[10] "The International Large Detector - DBD". http://ific.uv.es/~fuster/DBD-Chapters/Chapter%204%20ILD.pdf.

[11] W. Kilian, T. Ohl, and J. Reuter, "WHIZARD: Simulating multi-particle processes at LHC and ILC" *Eur.Phys.J.* **C21** (2011) 1742, arXiv:0708.4233 [hep-ph].

[12] M. Moretti, T. Ohl, and J. Reuter, "O'mega: An optimizing matrix element generator"
arXiv:hep-ph/0102195-rev.

[13] P. Doublet, *Hadrons in a highly granular SiW ECAL - Top quark production at the ILC*. PhD
thesis, Laboratoire de l'Accélérateur Linéaire and Université Paris Sud - Paris XI, 2011.
http://tel.archives-ouvertes.fr/tel-00657967.

[14] P. Doublet, F. Richard, T. Frisson, R. Pöschl, and J. Rouëné, "Determination of Top-quark
Asymmetries at the ILC".

[15] I. Garcìa Garcìa, "Top quark studies at a Linear Collider" Master's thesis, Universitat de
Valencia, 2012. http://digital.csic.es/handle/10261/64306.

[16] E. Barger *et al.*, "The Top Quark Production Asymmetries A_{FB}^t and A_{FB}^ℓ" *Phys.Rev.Lett.*
108 (2012) , arxiv:1201.1790 [hep-ph].

[17] C. Rimbault, P. Bambade, K. Mönig, and D. Schulte, "Impact of beam-beam effects on
precision luminosity measurements at the ILC" *LAL 07-157, EUROTEV-Report-2007-017*
(2007) . http://publication.lal.in2p3.fr/2007/lal07157.pdf.

[18] A. Rosca, "Measurement of the beam polarisation at the ILC using the WW annihilation
data" *LC-REP-2013-009* .
http://www-flc.desy.de/lcnotes/notes/LC-REP-2013-009.pdf.

[19] J. Fleischer, A. Leike, T. Riemann, and A. Werthenbach, "Elektroweak one-loop corrections
for e^+e^- annihilation into $t\bar{t}$ including hard bremsstrahlung" *Eur.Phys.J.* **C31** (2003) 37,
arXiv:hep-ph/0302259.

[20] E. Glover *et al.*, "Top quark physics at colliders" *ActaPhys.Polon.* **B35** (2004) 2671,
arXiv:hep-ph/0410110.

[21] J. A. Aguilar-Saavedra, M. C. N. Fiolhais, and A. Onofre, "Top effective operators at the
ILC" arXiv:1206.1033 [hep-ph].

[22] L. Randall and R. Sundrum, "A large mass hierarchy from a small extra dimension"
Phys.Rev.Lett. **83** (1999) 3370, arXiv:9905221 [hep-ph].

[23] A. Djouadi, G. Moreau, and F. Richard, "Resolving the A_{FB}^b puzzle in an extra dimensional
model with an extended gauge structure" *Nucl.Phys.* **B773** (2007) 43,
arXiv:hep-ph/0610173.

[24] A. Djouadi, J. Moreau, F. Richard, and R. K. Singh, "The forward-backward asymmetry of
top quark production at the Tevatron in warped extra dimensional models" *Phys.Rev.* **D82**
(2010) 071702, arXiv:0906.0604 [hep-ph].

[25] A. Djouadi, J. Moreau, F. Richard, and R. Singh, "Forward-backward asymmetries of the
bottom and top quarks in warped extra-dimensional models: LHC predictions from the LEP
and Tevatron anomalies" *Phys.Lett.* **B701** (2011) 458, arXiv:1105.3158 [hep-ph].

[26] A. G. Grozin, P. Marquard, J. H. Piclum, and M. Steinhauser, "Three-Loop Chromomagnetic
Interaction in HQET" *Nucl.Phys.* **B789** (2008) 277, arXiv:0707.1388 [hep-ph].

[27] L. Labun and J. Rafelski, "Top anomalous magnetic moment and the two photon decay of
Higgs" arXiv:arXiv:1209.1046 [hep-ph].